High-Temperature Co-Electrolysis: A Versatile Method to Sustainably Produce Tailored Syngas Compositions

Lucy Dittrich,[1,2,z] Markus Nohl,[1,2] Esther E. Jaekel,[1,2] Severin Foit,[1] L.G.J. (Bert) de Haart,[1,*] and Rüdiger-A. Eichel[1,2]

[1] *Institut für Energie- und Klimaforschung (IEK-9), Forschungszentrum Jülich 52425 Jülich, Germany*
[2] *Institut für Physikalische Chemie, RWTH Aachen University, Germany*

High-temperature co-electrolysis of carbon dioxide and steam is a promising method to produce 'white' syngas by making use of renewable energy and carbon dioxide as sustainable feedstock. The technological key advantage is the possibility to tailor syngas compositions over a broad range. This paper presents a systematic investigation of the syngas tailoring process by establishing relationships between feed gas compositions and flow rates to the syngas ratio. A linear dependence between the H_2O:CO_2 ratio in the feed gas and the H_2:CO ratio in the output gas was observed. Furthermore, the syngas ratio remains mostly invariant upon variations in electrochemical potential and fluctuating gas utilizations/flow rates during operation of a co-electrolysis cell. Most importantly, the co-electrolysis performance was demonstrated to operate at high current densities of up to 3.2 A·cm^{-2} over a broad range of feed gas compositions with faradaic efficiencies of nearly 100%. The possibility to operate co-electrolysis under transient load conditions renders this method particularly suitable in future scenarios of intermittent availability of renewables. The results described here illustrate the versatility of co-electrolysis, which can produce all relevant syngas compositions in a single-step process at constantly high performance.

 [DOI: 10.1149/2.0581913jes]

Manuscript submitted July 10, 2019; revised manuscript received August 5, 2019. Published August 22, 2019.

The industry sector worldwide is responsible for 13.14 Gt CO_2/yr of climate-wrecking CO_2 emissions.[1] A highly promising CO_2 valorization technology is the co-electrolysis of (waste) water and carbon dioxide to form hydrogen and carbon monoxide – i.e. syngas – in a 'Power-to-Syngas' scenario.[2–5] This scenario relies on replacing the currently used technologies to produce 'gray' syngas based on fossil resources, by co-electrolysis to obtain 'white' syngas. Downstream Syngas Chemistry is a well-established branch in chemical industry. Syngas can be converted to a diverse range of chemical base products by subsequent catalytic reactions.[6–9] This diversity is obtained by varying the H_2:CO ratio, which typically ranges from 1:1 to 3:1.

The advantage of high-temperature co-electrolysis is the tailoring of the syngas ratio in a single process step by adjusting the operating parameters. Figure 1 schematically shows the path from co-electrolysis of different H_2O:CO_2 ratios toward different products and their applications based on the content of carbon, hydrogen and oxygen. For synfuels, for example, which only contain carbon and hydrogen, H_2:CO ratios between 2:1 and 3:1 are used. Aldehydes and ethers for chemical industry include oxygen and therefore need a higher CO content in the syngas mixture. In future energy scenarios, electrochemical technologies have to meet various objectives, which include not only highly efficient conversion and low aging rates, but also the ability to operate in transient mode as function of fluctuating availability of renewables. From an economic perspective, CAPEX requires slow aging rates, whereas high current densities are advantageous for both, low OPEX and CAPEX, which is in line with the objective related to operation in transient mode.

The solid oxide cell (SOC) technology, which was developed in the last decades to a near-commercial state,[10–13] fulfills most of these criteria. With the development of anode supported cells, high current densities at moderate operating temperatures (< 800°C) can be achieved.[14,15] The Solid Oxide Electrolysis Cell (SOEC) technology can be typically operated above 1 A·cm^{-2}.[16–18] The aging rate (i.e. decrease in cell potential) under constant load operation and hydrogen as fuel typically lies below 0.3% per 1000 h.[19,20] The underlying processes, responsible for degradation in solid oxide fuel cells (SOFC), are mostly understood[21–23] or can be described by a most recently developed quantitative model.[24] For the operation in co-electrolysis mode and under transient mode of operation, however, the durability has not yet been investigated sufficiently.

Co-electrolysis can be performed at either high[25–33] or low[34,35] temperatures. The high-temperature co-electrolysis makes use of the available SOC technology. During high-temperature co-electrolysis three main reactions are possible at the fuel electrode: the electrochemical conversions of steam to hydrogen and of carbon dioxide to carbon monoxide, as well as the reverse water gas shift (RWGS) equilibrium. In literature, there is currently no clear consent for whether the carbon dioxide is only converted in the RWGS equilibrium or electrochemically as well. The results of Stoots et al.[36] point toward a CO conversion by RWGS exclusively, while the results of Ebbesen et al.[26] show that the electrochemical conversion of CO_2 also occurs.

$$H_2O + 2e^- \rightarrow H_2 + O^{2-} \quad (1)\ \text{steam reduction}$$

$$CO_2 + 2e^- \rightarrow CO + O^{2-} \quad (2)\ CO_2\ \text{reduction}$$

$$H_2 + CO_2 \rightleftharpoons CO + H_2O \quad (3)\ (R)\ \text{WGS reaction}$$

Here, we describe a systematic investigation of co-electrolysis to produce tailor-made syngas compositions under varying current density.

Experimental

The experiments were performed using commercially available cathode-supported full cells from CeramTec. These cells have a diameter of 2 cm and an active area of 0.79 cm^2. The cells consist of a Ni/YSZ (yttria-stabilized zirconia) cathode, an YSZ electrolyte, a CGO (cerium gadolinium oxide) barrier layer and an LSCF (lanthanum strontium cobalt ferrite) anode. The cells were placed in a Probostat sample holder (Norwegian Electro Ceramics AS, NorECs) as described previously.[22] The cell is contacted on the air side with a platinum current collector and on the fuel side with a nickel mesh. The cathode and anode gas chambers are separated by ceramic tubes to which the cell is sealed with a gold ring. The gases on the fuel side (CO, H_2, CO_2, N_2) are led through a water bath to adjust the water content based on the temperature dependence of the vapor pressure. The NiO in the cathode of the as-bought cells was reduced with H_2 at 900°C during the first heating of the cells. To prevent reoxidation

*Electrochemical Society Member.
[z]E-mail: l.dittrich@fz-juelich.de

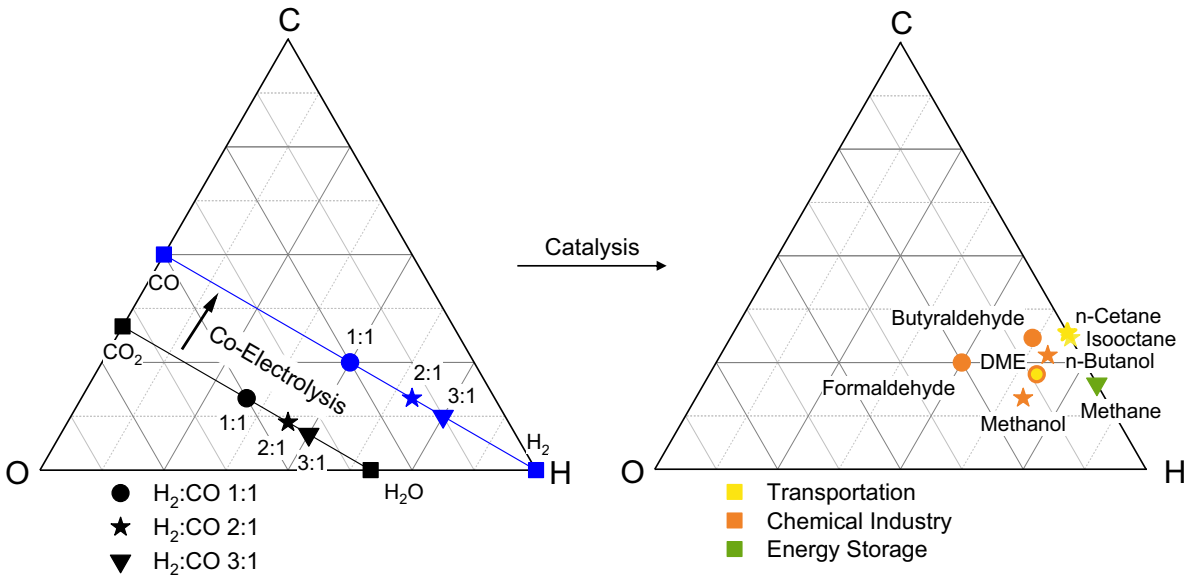

Figure 1. Schematic representation of Power-to-X applying co-electrolysis to produce syngas as reaction intermediate.

of the Nickel, hydrogen is constantly fed to the cathode. The electrochemical tests were performed only up to a maximum voltage of 1.4 V to keep the degradation effects that might occur at high voltages as low as possible. To ensure comparability among different cells the current density data was normalized to fit the real contacted area (see supporting info).

For the tailoring experiments a current-voltage curve (i/V curve) with a scan rate of 1 $mA{\cdot}s^{-1}$ from OCV to 1.4 V was performed and the output gas composition was measured with a mass spectrometer which collects data every 1.7 s. For the investigation of feed gas compositions, these experiments were conducted at 900°C and 6 $l{\cdot}h^{-1}$ comparing feed gas compositions of 40% H_2O + 20% H_2 and varied CO_2 content (40%, 20%, 13%; balanced with N_2). For the investigation of the influence of flow rate, rates of 6, 3, 2 and 1 $l{\cdot}h^{-1}$ were compared at 900°C for the feed gas composition of 40% H_2O + 40% CO_2 + 20% H_2.

The theoretical model for calculating the output gas composition is based on thermodynamics. The composition is calculated in a three-step process. Firstly, the equilibrium composition is determined iteratively by a self-written equilibrium solver in python using the package "chempy"[37] with cross-checked results. The thermodynamic data was taken from the Ivtanthermo database. For the following electrolysis step, the change of composition for each respective current density was calculated according to Faraday's law. Lastly, a second equilibrium step is performed with the modified composition after electrolysis as explained above.

The performance was tested by measuring i/V curves in electrolysis mode from open cell voltage (OCV) to 1.4 V with a scan rate of 10 $mA{\cdot}s^{-1}$. These experiments were performed using the Potentiostat Vertex.5A by Ivium Technologies. Various fuel gas compositions were compared: Co-electrolysis was tested with gas mixtures of 80% fuel and 20% hydrogen, where the fuel consisted of water and carbon dioxide in the ratios ranging from 3:1 to 1:3. The performance was also tested for mixtures of 50% CO_2 + 50% CO (pure carbon dioxide electrolysis), 50% H_2O + 50% H_2 (pure steam electrolysis), 50% CO_2 + 50% H_2 and 25% H_2O + 25% CO_2 + 50% H_2 (co-electrolysis). From the i/V curves the area specific resistances were obtained by numerical derivation with Origin by OriginLab.

Results and Discussion

To demonstrate the viability of co-electrolysis to generate tailored 'white' syngas compositions of H_2:CO in the range necessary for following-up syngas chemistry,[2–5] several H_2O:CO_2 feed gas compositions and flow rates at varying current densities have been monitored by mass spectrometry. The obtained data do not show any other products than hydrogen and carbon monoxide leading to a faradaic efficiency (ratio of measured to theoretically possible amount of syngas) of around 100%.

To compare H_2O:CO_2 ratios in the feed gas, compositions of 40% H_2O, 20% H_2 and varied CO_2 content (40%, 20%, 13% balanced with N_2), i.e. H_2O:CO_2 ratios of 1:1, 2:1 and 3:1, were fed to the fuel electrode with a flow rate of 6 $l{\cdot}h^{-1}$. A constant flow of 6 $l{\cdot}h^{-1}$ of air was fed to the air electrode. The hydrogen in the fuel feed gas is necessary to prevent oxidation of the Nickel cathode.

The obtained volume fractions of the fuel gases as a function of the current density are shown in Figures 2a–2c. The initial measured gas composition at open cell voltage (OCV, i = 0 $A{\cdot}cm^{-2}$) already differed from the input composition regulated by mass flow controllers (MFCs). The difference is explained by the RWGS taking place at the operating temperature of 900°C in the presence of a catalyst (Ni). The equilibrium compositions are shown in Table I.

In Figure 2 the feed gas composition is shown on the y-axis. Starting at 0 $A{\cdot}cm^{-2}$, the measured composition is plotted. Decreasing the CO_2 content decreases the total fuel content. The resulting higher fuel utilization at the same current density causes supply limitations.

Table I. Equilibrium compositions at 900°C of the investigated inlet gas streams (balanced with N_2).

Feed gas composition $H_2O + CO_2 + H_2 + CO$ [%]	Equilibrium gas composition $H_2O + CO_2 + H_2 + CO$ [%]
50 + 0 + 50 + 0	50 + 0 + 50 + 0
0 + 50 + 50 + 0	26.5 + 23.5 + 23.5 + 26.5
0 + 50 + 0 + 50	0 + 50 + 0 + 50
25 + 25 + 50 + 0	38.6 + 11.4 + 36.4 + 13.6
60 + 20 + 20 + 0	64.6 + 15.4 + 15.4 + 4.6
53 + 27 + 20 + 0	59.4 + 20.6 + 13.9 + 6.1
40 + 40 + 20 + 0	48.9 + 31.1 + 11.1 + 8.9
27 + 53 + 20 + 0	38.3 + 41.7 + 8.4 + 11.6
20 + 60 + 20 + 0	32.9 + 47.1 + 7.1 + 12.9
40 + 20 + 20 + 0	45.7 + 14.3 + 14.3 + 5.7
40 + 13.3 + 20 + 0	44.1 + 9.2 + 15.9 + 4.1
5 + 75 + 20 + 0	20.7 + 59.3 + 4.3 + 15.7
0 + 80 + 20 + 0	16.6 + 63.4 + 3.4 + 16.6
0 + 80 + 5 + 0	4.8 + 75.4 + 0.2 + 4.8

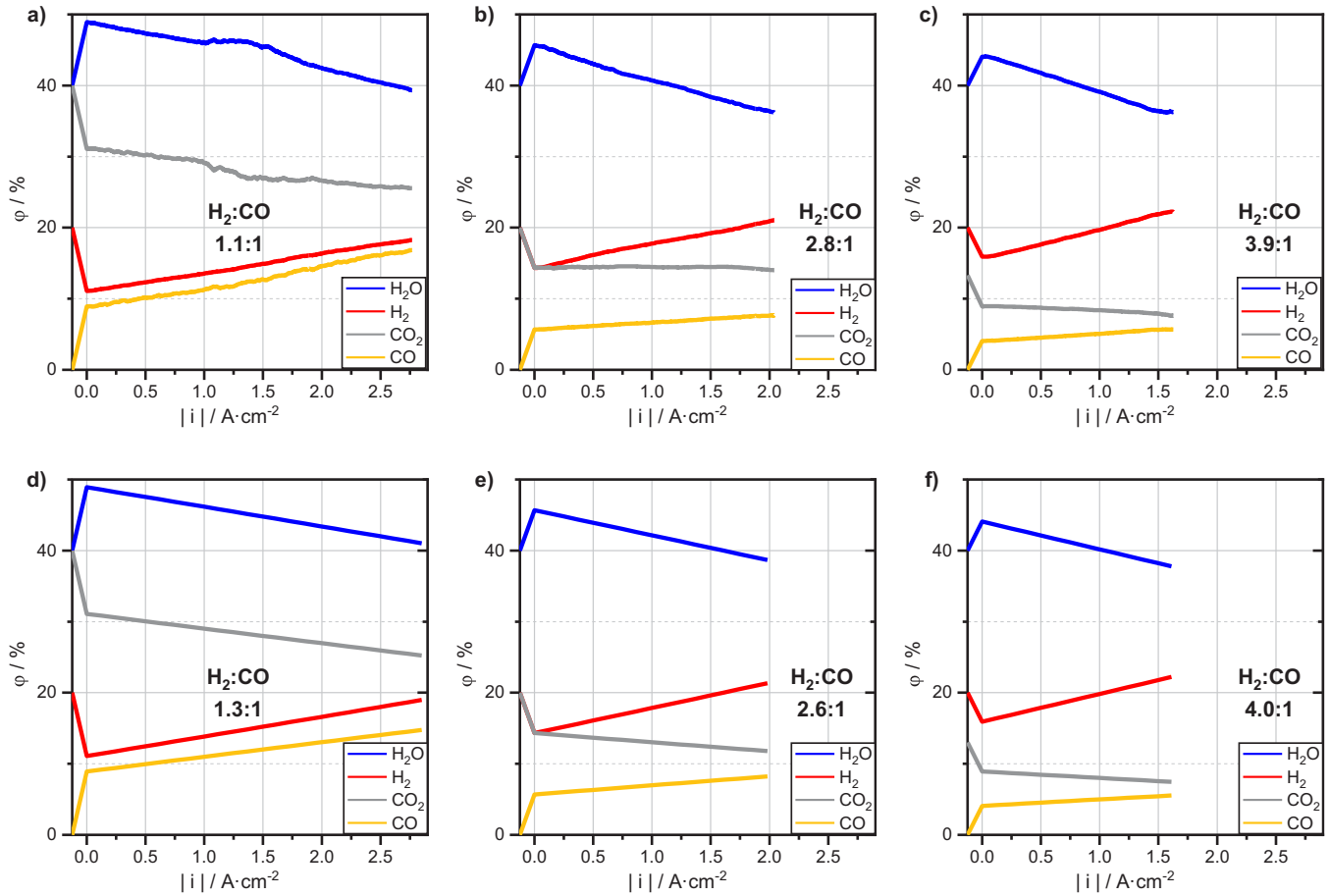

Figure 2. Experimental (a-c) and theoretical (d-f) product gas composition as function of the current density. Compared are the initial compositions of 40% H_2O + 40% CO_2 + 20% H_2 (left), 40% H_2O + 20% CO_2 + 20% H_2 + 20% N_2 (middle) and 40% H_2O + 13% CO_2 + 20% H_2 + 27% N_2 (right) at 900°C and 6 l·h^{-1}. The experiments were conducted up to a potential of 1.4 V causing the differing current density limits. Displayed on the y-axis is the feed gas composition. Starting at 0 A·cm^{-2}, the equilibrium composition is shown, which differs from the feed gas composition due to RWGS at operating temperature.

Hence, the current density that is reached at our chosen maximum of 1.4 V (see experimental section) decreases. Therefore, the curves in Figures 2b and 2c end at lower current densities than the one in Figure 2a.

With no applied current, only the RWGS converts the CO_2 to CO. For the gas mixture with 40% H_2O + 40% CO_2 + 20% H_2, the equilibrium composition is 48.9% H_2O + 31.1% CO_2 + 11.1% H_2 + 8.9% CO. Thus, 22% of CO_2 is already converted by RWGS. Increasing the current density to 2.5 A·cm^{-2}, the conversion of CO_2 increases to 36%. Thus, increasing the current and performing co-electrolysis increases the syngas yield compared to the sole RWGS equilibrium.

The obtained syngas composition slightly changes with current density. For the compared feed gas compositions at 6 l·h^{-1} the H_2:CO ratio slightly increases with increasing current density. This increase is stronger for the compositions with reduced CO_2 content. Overall the syngas ratio is in alignment with the H_2O:CO_2 ratio in the feed gas stream.

For the investigation of the influence of flow rates (i.e. fuel utilization), a gas mixture of 40% H_2O + 40% CO_2 + 20% H_2 was fed to the fuel electrode with 6, 3, 2 or 1 l·h^{-1} (Figure S1 in supporting info). The air side was supplied with air with the same respective flow rate. The flow rates correspond to gas velocities of $7.6 \cdot 10^3$, $3.8 \cdot 10^3$, $2.5 \cdot 10^3$ and $1.3 \cdot 10^3$ cm·h^{-1}, respectively, by dividing by the active surface area of the cell.

The decrease of the flow rate causes an increase in (maximum) gas utilization at 1.4 V from 15% for 6 l·h^{-1} to 45% for 1 l·h^{-1}. At any given current density the absolute amount of converted molecules per second is determined by Faraday's law. Since this is only dependent on the applied current density, decreasing the flow rate means that a higher percentage of that feed gas is converted (more feed gas is utilized). Decreased flow rates also lead to a reduced current density at 1.4 V. The syngas ratio, however, is not significantly affected by the flow rate in the experimentally obtained gas output. Only a slight shift toward CO is observed for lower flow rates.

To further analyze the experimental observations, thermodynamic calculations of the product gas compositions were conducted. These calculations are based on the assumption of infinitely fast kinetics and follow the below-mentioned procedure for each selected current density. Firstly, an equilibrium composition of the feed is determined. Secondly, the applied current density determines the amount of electrolyzed H_2O or CO_2 according to ideal Faraday's law. Thirdly, the equilibrium composition after electrolysis is calculated again.

Theoretically, the final composition is independent on the type of electrolysis, H_2O or CO_2, if only thermodynamics is considered. Calculations with steam electrolysis led to the same output compositions as with carbon dioxide electrolysis. The output composition therefore depends on the total conversion and RWGS equilibrium. The composition of the input gas also influences the equilibrium.

The theoretically determined compositions are plotted in Figures 2d–2f and are well in line with the experimental data. Here as well an increase in H_2:CO ratio with increasing current density is observed. This effect is therefore caused by the input gas composition and the influence on the RWGS equilibrium. Calculations with lower hydrogen content for example show a reduced increase of H_2:CO ratio. Only for the water content the agreement is rather weak. In the experiment it decreases significantly stronger than in theory. This might be

Table II. Area specific resistance at 0.5 A·cm^{-2} and current density at maximum potential of 1.4 V for various feed gas compositions (balanced with N_2).

Composition $H_2O + CO_2 + H_2 + CO$ [%]	$ASR_{0.5\ A\cdot cm\text{-}2}$[Ω·cm^2]	$\lvert i\rvert_{1.4\ V}$[A·cm^{-2}]	OCV_{exp}[V]	OCV_{theo}[V]
50 + 0 + 50 + 0	0.16	2.20	0.92	0.91
0 + 50 + 50 + 0	0.18	2.04	0.92	0.90
0 + 50 + 0 + 50	0.21	1.71	0.90	0.90
25 + 25 + 50 + 0	0.16	2.22	0.92	0.91
60 + 20 + 20 + 0	0.14	3.32	0.87	0.84
53 + 27 + 20 + 0	0.14	3.23	0.86	0.84
40 + 40 + 20 + 0	0.14	3.30	0.85	0.83
27 + 53 + 20 + 0	0.15	3.06	0.85	0.83
20 + 60 + 20 + 0	0.14	3.17	0.85	0.83
5 + 75 + 20 + 0	0.18	1.93	0.87	0.83
0 + 80 + 20 + 0	0.19	2.06	0.85	0.83
0 + 80 + 5 + 0	0.29	1.65	0.79	0.75

due to the missing kinetics, side reactions or adsorption effects in the theoretical model.

Significant deviations are observed in the H_2 content for lower flow rates (≤ 3 l·h^{-1}). While the experiment shows a H_2-fraction of 18% at i = 1 A·cm^{-2}, thermodynamics predicts a value of 27%. Tentatively, this deviation may be explained by kinetic effects, such as the residence time of molecules on electrode surfaces, as well as their ad- and desorption. If the CO_2 content is lowered and product gas compositions are compared, at higher flow rates (≥ 6 l·h^{-1}) the experimental values are consistent to the thermodynamic calculations.

The electrochemical performance of co-electrolysis – i.e. the efficiency at which renewables are fed into the electrochemical conversion process – was investigated by direct current (dc) measurements at different gas compositions. From the obtained i/V curves the open circuit voltage (OCV), the area specific resistance (ASR) at 0.5 A·cm^{-2} and the current density at the chosen maximum voltage of 1.4 V were determined. The experimentally measured OCVs for the compared compositions deviate from the theoretically calculated values (Table II) by about 4 – 40 mV (0.4 – 5%). For the H_2O/H_2 mixture, for example, an OCV of 0.92 V was observed, while the calculated Nernst-Potential is 0.91 V. This is a deviation of 1.2%. These small deviations are due to nearly unavoidable leakages from the cell setup. However, since all measurements on the same cell are affected in the same way, the observed trends should not be falsified.

High-temperature 'pure' steam and carbon dioxide electrolysis with fuel compositions of 50% H_2O + 50% H_2 and 50% CO_2 + 50% CO, respectively, were used as reference. The corresponding comparison of electrochemical performance for co-electrolysis with a fuel composition of 25% H_2O + 25% CO_2 + 50% H_2 is depicted in Figure 3. The RWGS causes this composition to equilibrate to 38.6% H_2O + 11.4% CO_2 + 36.4% H_2 + 13.6% CO. This means that the RWGS already converts more than half of the CO_2 already at 0 A·cm^{-2}. The equilibrium mixture therefore contains almost four times more H_2O than CO_2. For this fuel composition, the co-electrolysis performance (ASR and current density at 1.4 V, Table II) is comparable to the electrochemical performance of steam electrolysis, allowing operation at current densities above 1 A·cm^{-2}.

Also shown in Figure 3 is the i/V curve for a fuel composition of 50% CO_2 + 50% H_2. The ASR of the CO_2 – H_2 mixture is situated between steam/co-electrolysis and CO_2 electrolysis with a tendency toward steam electrolysis. This behavior can also be explained by the RWGS that causes the mixture of 50% CO_2 + 50% H_2 to equilibrate to about equal amounts of CO_2, H_2, H_2O and CO at the operating temperature already at OCV (see Table II).

Literature already states that the ASR of pure H_2O electrolysis (H_2O/H_2 mixture) is lower than that of pure CO_2 electrolysis (CO_2/CO mixture).[26,36] This is observed here as well. Moreover, the ASR of the co-electrolysis mixture is identical to the H_2O electrolysis, which supports the recent hypothesis by Stoots et al.[36] that during co-electrolysis the carbon dioxide preferably reacts in the RWGS reaction with the hydrogen that is produced by steam electrolysis, producing steam and carbon monoxide. To investigate whether this is the case for all H_2O:CO_2 ratios and thus draw conclusions about a possible mechanism several feed gas compositions were compared.

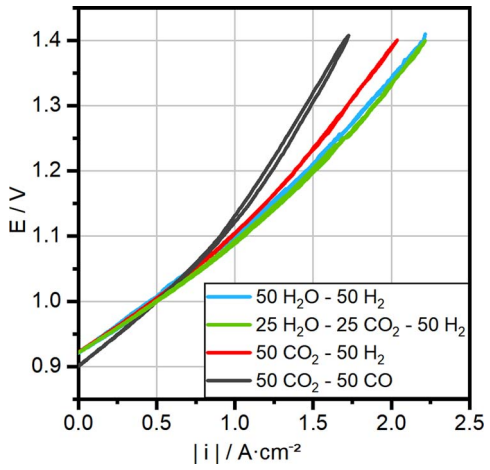

Figure 3. i/V curves of different compositions. Compared are 50% H_2O + 50% H_2, 50% CO_2 + 50% CO, 50% CO_2 + 50% H_2 and 25% H_2O + 25% CO_2 + 50% H_2 at 900°C and 6 l·h^{-1}.

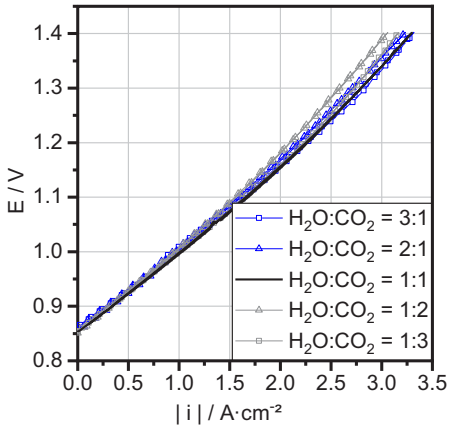

Figure 4. i/V curves of different compositions. Compared are compositions containing 80% fuel with H_2O:CO_2 ratios of 3:1 to 1:3 and 20% H_2 at 900°C and 6 l·h^{-1}.

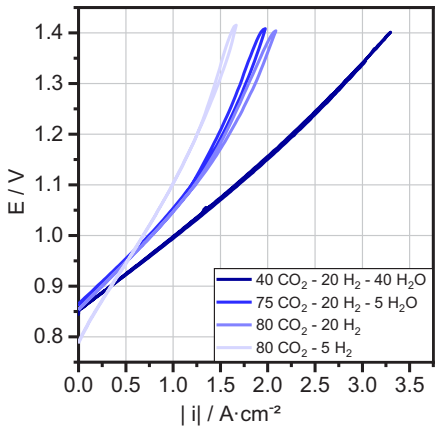

Figure 5. i/V curves of different compositions with low H_2O content. Compared are 40% H_2O + 40% CO_2 + 20% H_2, 5% H_2O + 75% CO_2 + 20% H_2, 80% CO_2 + 20% H_2 and 80% CO_2 + 5% H_2 + 15% N_2 at 900°C and 6 l·h^{-1}.

First, dc measurements of H_2O:CO_2 ratios of 3:1 to 1:3 at a constant fuel content of 80% have been investigated. The resulting syngas compositions include the most commonly used ratios of H_2:CO of 1:1, 2:1 and 3:1. The results show that the performance is not influenced by the feed gas ratio of H_2O:CO_2 in the investigated range (Figure 4). This effect can be seen in the graphs, which are almost identical, as well as in the area specific resistance (ASR) at 0.5 A·cm^{-2} and current density at 1.4 V (Table II). The ASR for all ratios is about 0.14 Ω·cm^2 and $i_{1.4\,V}$ is around 3.2 A·cm^{-2}. This confirms the dominance of steam electrolysis in the range of 64.6% H_2O + 15.4% CO_2 to 32.9% H_2O + 47.1% CO_2 (equilibrium composition of the fuel content of the 3:1 and 1:3 H_2O:CO_2 feed gas mixtures) as explained before.

The performance has also been investigated at low steam content to test the boundaries of co-electrolysis and find out at which point CO_2 electrolysis starts to be significant. The i/V curve results are shown in Figure 5 with the respective parameters in Table II. The equilibrium compositions show H_2O contents from 20% down to 5%. By lowering the steam content to 5%, the ASR starts to rise significantly from 0.18 Ω·cm^2 to 0.29 Ω·cm^2. Even the values for around 20% H_2O are slightly higher than those for the mixtures with >30% H_2O content. Since according to literature[26,36] the CO_2 electrolysis is slower and shows a significantly higher ASR than the H_2O electrolysis, it can be concluded that for low H_2O contents the CO_2 is not only converted in the RWGS, but also electrolyzed. Thus, CO_2 electrolysis seems to become significant for H_2O contents of < 20% in the equilibrium gas mixture.

Conclusions

In summary, co-electrolysis not only provides a valorization option for the greenhouse gas CO_2 by making use of renewable power sources, it can also be used to produce all relevant syngas ratios at will and with the same power input. We were able to show that the tailoring of specific syngas ratios is possible in one electrolysis step by adjusting the H_2O:CO_2 ratio in the feed gas stream. The resulting syngas composition is in alignment with its corresponding ratio of the feed gas with a slight surplus of H_2 for the investigated compositions. The syngas composition is invariant to the applied current density, which means that co-electrolysis is suitable for transient conditions of renewable energy sources. Compared to low temperature electrolysis, which shows current densities of up to 300 mA·cm^{-2},[34] we were able to produce syngas at current densities of up to 3.2 A·cm^{-2} (within our self-given potential limitation of 1.4 V) and faradaic efficiencies of almost 100%. The stability of the co-electrolysis process is currently under investigation. With electrochemical cells that are stable above 1.4 V even higher current densities and therefore increased space time conversion rates are possible.

Acknowledgments

The authors gratefully acknowledge funding by the German Federal Ministry of Education and Research (BMBF) within the Kopernikus Project P2X: Flexible use of renewable resources – research, validation and implementation of 'Power-to-X' concepts.

ORCID

Lucy Dittrich https://orcid.org/0000-0001-9255-9706

References

1. M. Fischedick, J. Roy, A. Abdel-Aziz, A. Acquaye, M. Allwood J., J.-P. Ceron, Y. Geng, H. Kheshgi, A. Lanza, D. Perczyk, L. Price, E. Santalla, C. Sheinbaum, and K. Tanaka, 2014: *Industry*, In: *Climate Change 2014: Mitigation of Climate Change. Contribution of Working Group III to the Fifth Assessment Report of the Intergovernmental Panel on Climate Change* [Edenhofer, O., R. Pichs-Madruga, Y. Sokona, E. Farahani, S. Kadner, K. Seyboth, A. Adler, I. Baum, S. Brunner, P. Eickemeier, B. Kriemann, J. Savolainen, S. Schlömer, C. von Stechow, T. Zwickel, and J. C. Minx, (eds.)]. Cambridge University Press, Cambridge, United Kingdom and New York, NY, USA (2014).
2. S. R. Foit, I. C. Vinke, L. G. J. de Haart, and R.-A. Eichel, *Angew. Chem., Int. Ed.*, **56**, 5402 (2017).
3. R. Schlögl, *ChemSusChem*, **3**, 209 (2010).
4. J. Artz, T. E. Müller, K. Thenert, J. Kleinkorte, R. Meys, A. Sternberg, A. Bardow, and W. Leitner, *Chem. Rev.*, **118**, 434 (2018).
5. M. Thema, M. Sterner, T. Lenck, and P. Götz, *Energy Procedia*, **99**, 392 (2016).
6. F. Fischer and H. Tropsch, *Ber. Dtsch. Chem. Ges. B*, **59**, 830 (1926).
7. C. Sun, P. Pfeifer, and R. Dittmeyer, *Chem. Eng. J.*, **326**, 37 (2017).
8. M. Haumann, K. Dentler, J. Joni, A. Riisager, and P. Wasserscheid, *Adv. Synth. Catal.*, **349**, 425 (2007).
9. K. Hackbarth, P. Haltenort, U. Arnold, and J. Sauer, *Chem. Ing. Tech.*, **90**, 1520 (2018).
10. N. Christiansen, S. Primdahl, M. Wandel, S. Ramousse, and A. Hagen, *ECS Trans.*, **57**(1), 43 (2013).
11. D. Schimanke, O. Posdziech, B. E. Mai, S. Kluge, T. Strohbach, and C. Wunderlich, *ECS Trans.*, **35**(1), 231 (2011).
12. O. Bucheli, M. Bertoldi, S. Modena, and A. V. Ravagni, *ECS Trans.*, **57**(1), 81 (2013).
13. B. Borglum and H. Ghezel-Ayagh, *ECS Trans.*, **57**(1), 61 (2013).
14. L. Blum, L. G. J. de Haart, J. Malzbender, N. H. Menzler, J. Remmel, and R. Steinberger-Wilckens, *J. Power Sources*, **241**, 477 (2013).
15. L. Blum, P. Batfalsky, Q. Fang, L. G. J. de Haart, J. Malzbender, N. Margaritis, N. H. Menzler, and R. Peters, *J. Electrochem. Soc.*, **162**, F1199 (2015).
16. M. A. Laguna-Bercero, *J. Power Sources*, **203**, 4 (2012).
17. J. B. Hansen, *Faraday Discuss.*, **182**, 9 (2015).
18. S. D. Ebbesen, S. H. Jensen, A. Hauch, and M. B. Mogensen, *Chem. Rev.*, **114**, 10697 (2014).
19. L. Blum, U. Packbier, I. C. Vinke, and L. G. J. de Haart, *Fuel Cells*, **4**, 646 (2013).
20. L. Blum, L. G. J. de Haart, J. Malzbender, N. Margaritis, and N. H. Menzler, *Energy technol.*, **4**, 939 (2016).
21. D. Roehrens, A. Neumann, A. Beez, I. C. Vinke, L. G. J. de Haart, and N. H. Menzler, *Ceramics Int.*, **42**, 9467 (2016).
22. K. Schiemann, V. Vibhu, S. Yildiz, I. C. Vinke, R. A. Eichel, and L. G. J. de Haart, *ECS Trans.*, **78**(1), 1027 (2017).
23. A. Beez, X. Yin, N. H. Menzler, R. Spatschek, and M. Bram, *J. Electrochem. Soc.*, **164**, F3028 (2017).
24. L. Kröll, L. G. J de Haart, I. C. Vinke, and R.-A. Eichel, *Phys. Rev. Appl.*, **7**, 044007 (2017).
25. S. D. Ebbesen, C. Graves, and M. Mogensen, *Int. J. Green Energy*, **6**, 646 (2009).
26. S. D. Ebbesen, R. Knibbe, and M. Mogensen, *J. Electrochem. Soc.*, **159**, F482 (2012).
27. S. R. Foit, L. Dittrich, V. Vibhu, I. C. Vinke, R-A. Eichel, and L. G. J. de Haart, *ECS Trans.*, **78**(1), 3139 (2017).
28. M. Torrell, S. Garcia-Rodriguez, A. Morata, G. Penelas, and A. Tarancon, *Faraday Discuss.*, **182**, 241 (2015).
29. Y. Zheng, J. Wang, B. Yu, W. Zhang, J. Chen, J. Qiao, and J. Zhang, *Chem. Soc. Rev.*, **46**, 1427 (2017).
30. R. Xing, Y. Wang, Y. Zhu, S. Liu, and C. Jin, *J. Power Sources*, **274**, 260 (2015).
31. L. Bernadet, J. Laurencin, G. Roux, D. Montinaro, F. Mauvy, and M. Reytier, *Electrochim. Acta*, **253**, 114 (2017).
32. S.-W. Kim, H. Kim, K. J. Yoon, J.-H. Lee, B.-K. Kim, W. Choi, J.-H. Lee, and J. Hong, *J. Power Sources*, **280**, 630 (2015).
33. Y. Wang, T. Liu, L. Lei, and F. Chen, *Fuel Process. Technol.*, **161**, 248 (2017).
34. T. Haas, R. Krause, R. Weber, M. Demler, and G. Schmid, *Nat. Catal.*, **1**, 32 (2018).
35. C. Delacourt, P. L. Ridgway, J. B. Kerr, and J. Newman, *J. Electrochem. Soc.*, **155**, B42 (2008).
36. C. M. Stoots, J. E. O'Brien, J. S. Herring, and J. J. Hartvigsen, *J. Fuel Cell Sci.Tech.*, **6**, 011014 (2009).
37. B. Dahlgren, *J. Open Source Softw.*, **3**, 565 (2018).